PNAS RESEARCH ARTICLE | CELL BIOLOGY OPEN ACCESS

Single p197 molecules of the mitochondrial genome segregation system of *Trypanosoma brucei* determine the distance between basal body and outer membrane

Salome Aeschlimann[a,b], Ana Kalichava[b,c], Bernd Schimanski[a], Bianca Manuela Berger[b,c], Clirim Jetishi[b,c], Philip Stettler[a,b], Torsten Ochsenreiter[c,1], and André Schneider[a,1]

Edited by Jodi Nunnari, University of California, Davis, CA; received March 10, 2022; accepted August 22, 2022

The tripartite attachment complex (TAC) couples the segregation of the single unit mitochondrial DNA of trypanosomes with the basal body (BB) of the flagellum. Here, we studied the architecture of the exclusion zone filament (EZF) of the TAC, the only known component of which is p197, that connects the BB with the mitochondrial outer membrane (OM). We show that p197 has three domains that are all essential for mitochondrial DNA inheritance. The C terminus of p197 interacts with the mature and probasal body (pro-BB), whereas its N terminus binds to the peripheral OM protein TAC65. The large central region of p197 has a high α-helical content and likely acts as a flexible spacer. Ultrastructure expansion microscopy (U-ExM) of cell lines exclusively expressing p197 versions of different lengths that contain both N- and C-terminal epitope tags demonstrates that full-length p197 alone can bridge the ∼270-nm distance between the BB and the cytosolic face of the OM. Thus U-ExM allows the localization of distinct domains within the same molecules and suggests that p197 is the TAC subunit most proximal to the BB. In addition, U-ExM revealed that p197 acts as a spacer molecule, as two shorter versions of p197, with the repeat domain either removed or replaced by the central domain of the *Trypanosoma cruzi* p197 ortholog reduced the distance between the BB and the OM in proportion to their predicted molecular weight.

Trypanosoma | kinetoplast DNA | mitochondrial genome | genome segregation | basal body

Replication and segregation of the mitochondrial DNA is essential for proper organellar function. While these processes have been studied in detail in yeast and mammals (1, 2), which represent most of the popular model systems for cell biology, we know much less about them in protozoans, which make up most of the eukaryotic diversity.

An especially interesting case is the parasitic protozoan *Trypanosoma brucei*. Unlike most other eukaryotes it has a single mitochondrion harboring only a single unit genome termed kinetoplastid DNA (kDNA) (3–6). It consists of two genetic elements, the maxicircles and the minicircles, which are topologically highly interlocked forming a disk-shaped network that is localized to a specific region within the mitochondrion opposite the basal body (BB) of the flagellum.

In contrast to the mitochondrial genomes of most other eukaryotes, the kDNA is replicated at a defined time point during the cell cycle just before the onset of the nuclear S phase (7, 8). Trypanosomes therefore require precise mechanisms for the segregation of the replicated kDNA, which guarantee that after binary fission of the mitochondrion (9), the two daughters receive one kDNA disk each. This is achieved by coupling kDNA segregation to the segregation of another single copy structure in trypanosomes, the BB of the flagellum (10).

This coupling requires a unique structure termed tripartite attachment complex (TAC), which physically connects the kDNA disk to the BB of the flagellum and thus determines the relative positions of two structures that reside in different compartments. Disruption of the TAC is lethal. It leads to overreplicated kDNA that cannot be segregated anymore, eventually resulting in daughter cells lacking kDNA (6, 11).

Most eukaryotic cells have many mitochondria, each containing multiple genomes called nucleoids (1). In these cases, the segregation of nucleoids during cell division can, at least in principle, occur stochastically. Thus, the precise mitochondrial genome segregation via the TAC is unique to trypanosomes and their relatives. However, intriguingly, the TAC shares features with the mammalian mitotic spindle that segregates nuclear chromosomes during cell division. Their organizing centers, the flagellar BB (for the TAC) and the centriole (for the spindle), are evolutionarily and structurally highly conserved (12). However, unlike the mitotic spindle in mammals, the TAC has

Significance

Segregation of the replicated single unit mitochondrial genome of *Trypanosoma brucei* requires a large hardwired structure that connects the organellar DNA with the flagellar basal body. The cytosolic part of this structure consists of filaments made of p197 molecules, a protein with a molecular weight of approximately 660 kDa. The N terminus of p197 is anchored to the peripheral mitochondrial outer membrane protein TAC65, whereas its C terminus connects to the base of the basal body. The large α-helical central domain of p197 consists of approximately 26 repeats each 175 aa in length. It provides a flexible spacer that connects the outer membrane with the basal body and determines the distance between the two structures.

Author affiliations: [a]Department of Chemistry, Biochemistry, and Pharmaceutical Sciences, University of Bern, Bern CH-3012, Switzerland; [b]Graduate School for Cellular and Biomedical Sciences, University of Bern, Bern CH-3012, Switzerland; and [c]Institute of Cell Biology, University of Bern, Bern CH-3012, Switzerland

Author contributions: S.A., A.K., B.S., T.O., and A.S. designed research; S.A., A.K., B.S., B.M.B., C.J., and P.S. performed research; S.A., A.K., B.S., B.M.B., C.J., T.O., and A.S. analyzed data; and S.A., T.O., and A.S. wrote the paper.

The authors declare no competing interest.

This article is a PNAS Direct Submission.

[1]To whom correspondence may be addressed. Email: torsten.ochsenreiter@unibe.ch or andre.schneider@unibe.ch.

This article contains supporting information online at http://www.pnas.org/lookup/suppl/doi:10.1073/pnas.2204294119/-/DCSupplemental.

Published September 26, 2022.

to cross two membranes before it can bind to the kDNA. Moreover, the concept of coupling inheritance of organelles to flagellar segregation also applies to mitosomes of the anaerobic protist *Giardia*. In these cells a subgroup of mitosomes is linked to the axonemes of the oldest flagella (13, 14). This indicates that a structure of unknown composition that is analogous to the part of the TAC that links the flagellum to the mitochondrial outer membrane (OM) might exist in *Giardia*.

The TAC has three morphologically defined subdomains: 1) the unilateral filaments (ULFs) that connect the kDNA to the mitochondrial inner membrane (IM), 2) the exclusion zone filaments (EZFs) between the BB of the flagellum and the OM, and 3) the differentiated membranes (DMs) that link the ULFs across the OM and IM with the EZFs (15). Due to the TAC, the median distance between the kDNA and the IM is fixed to ∼100 nm and the one between the OM and the BB to about 270 nm. The latter distance is bridged by the EZFs, whose precise architecture and length determination are presently unknown.

In recent years many essential components of the different TAC subdomains have been identified. The ULF region was shown to consist of p166, the first TAC component identified (16), which also connects to the IM (17), and TAC102, which localizes close to the kDNA (18). Counterintuitively, the DMs, the smallest subregion of the TAC, has the most complex composition. In the OM alone four different integral membrane proteins (TAC60, TAC40, TAC42, and pATOM36) as well as TAC65, a peripherally OM-associated protein that faces the cytosol, have been identified (19, 20). Moreover, pATOM36 in addition to its role in the TAC is also involved in the biogenesis of OM proteins (21–23). In contrast, p166 is the only known TAC subunit that is anchored in the mitochondrial IM (17). The EZF subdomain of the TAC finally consists of at least one essential factor: p197, which is the focus of the present study (24).

Unlike for other mitochondrial protein complexes, we find only a single TAC structure in the mitochondrion of nondividing cells (15). The overarching principle of TAC biogenesis is a hierarchical assembly starting from the BB of the flagellum progressing toward the kDNA (25).

A prerequisite to build a precise model of the TAC and to understand how the structure is assembled requires information about how each TAC component is arranged within the structure and how it interacts with which other TAC components. Here we provide this information for p197, the largest TAC component. According to TriTrypDB p197 has a predicted molecular mass of 197 kDa and contains 3.5 tandem repeats of 175 identical amino acids. However, as discussed below its true molecular mass is likely much larger. Using molecular genetics and in vivo complementation assays, involving differentially tagged p197 variants combined with ultrastructure expansion microscopy (U-ExM), we show which domains of p197 are essential for localization and/or function of p197. We demonstrate how p197 is arranged in the EZF region and identify its interaction partner in the periphery of the OM. Finally, we show that individual p197 molecules form and determine the length of the EZFs.

Results

p197-HA Is Functional and Localizes to Both Mature and Pro-BBs. To investigate the role of p197 in the TAC, we produced an RNAi cell line targeting the 3′ untranslated region (UTR) of p197 (p197 3′ UTR RNAi) (for a list of cell lines used in this study see *SI Appendix*, Table S1). In this cell line, induction of RNAi strongly interferes with normal growth and causes mis-segregation of the kDNA resulting in cells that either lack kDNA or contain overreplicated kDNA networks (*SI Appendix*, Fig. S1*A*). This is in agreement with previous studies (24) and corresponds to the typical phenotype of cell lines that are deficient for TAC subunits (11). Since RNAi targets the 3′ UTR of the p197 mRNA its open-reading frame (ORF) is not affected. Thus, we used the p197 3′ UTR RNAi cell line and in situ HA-tagged one of its p197 alleles at the C terminus. (Note that the tagging replaces the endogenous 3′ UTR). Addition of tetracycline (Tet) to this cell line, termed p197 3′ UTR RNAi + p197-HA, shows that expression of the RNAi-resistant p197-HA version restores normal growth and kDNA segregation, indicating that the C-terminal HA tag does not interfere with p197 function (*SI Appendix*, Fig. S1*B*).

Subsequently, immunofluorescence (IF) analysis of detergent-extracted cytoskeletons was used to compare the localization of p197-HA with the trypanosomal SAS-6 homolog (*SI Appendix*, Fig. S2). SAS-6 is an evolutionary conserved protein and has been implicated in the assembly of the centriole cartwheel (26). In *T. brucei*, SAS-6 localizes to both the mature BB as well as the pro-BB throughout the cell cycle (27–29).

In interphase cells, with one kDNA (K) and one nucleus (N), a configuration termed 1K1N, both proteins colocalize at two closely opposed dots that correspond to the mature BB and the pro-BB (*SI Appendix*, Fig. S2 *A*, *Top* row), respectively. Further into the cell cycle, when the kDNA has been duplicated but not yet segregated (configuration: dK1N), the two proteins localize to three adjacent dots in most cells, likely corresponding to the mature BB and pro-BB of the old flagellum and the new mature BB of the new flagellum (*SI Appendix*, Fig. S2*A*, second row). Finally, two dots each of p197 and SAS-6 are detected for each kDNA in cells showing 2K1N and 2K2N configurations (*SI Appendix*, Fig. S2*A*, last two rows). Thus, p197-HA colocalizes with SAS-6 throughout the cell cycle, indicating that assembly of the TAC starts simultaneously with the formation of the pro-BB and thus precedes the growth of the new flagellum as has been reported recently (30).

p197 Localizes to the Bottom of the BB surrounding SAS-6. To analyze the intracellular localization of p197-HA more precisely we used U-ExM, which was established for trypanosomes recently (31–33). U-ExM allows the increase of the spatial resolution for microscopic imaging by physical expansion of the cell (34, 35). Fig. 1*A* shows the cellular region of *T. brucei* that contains the BBs and the kDNAs. It is stained for p197-HA and α-tubulin using the antibody AA345 (36), which detects the mature and pro-BB (25, 37). The resolution of the pictures is greatly increased when compared to conventional IF microscopy. As expected for the mature and the pro-BB, the α-tubulin signals are consistent with a hollow cylindrical structure, which is viewed either from the top, the bottom, or from the side. p197 is detected adjacent to the bottom layer of the mature BB and the pro-BB and seems to form a partial ring that extends the hollow cylinder defined by the 9 microtubule triplets of the BB. The U-ExM in Fig. 1*B* shows that, in agreement with its proposed function in cartwheel assembly, SAS-6 appears to localize to the center of the partial ring defined by p197 (31). In summary, these results suggest that p197 is the TAC subunit that is most proximal to the mature BB and the pro-BB.

The C Terminus of p197 Is Anchored at the BB. Next we complemented the p197 3′ UTR RNAi cell line with a Tet-inducible C-terminal HA-tagged p197 variant lacking the N-terminal 1228

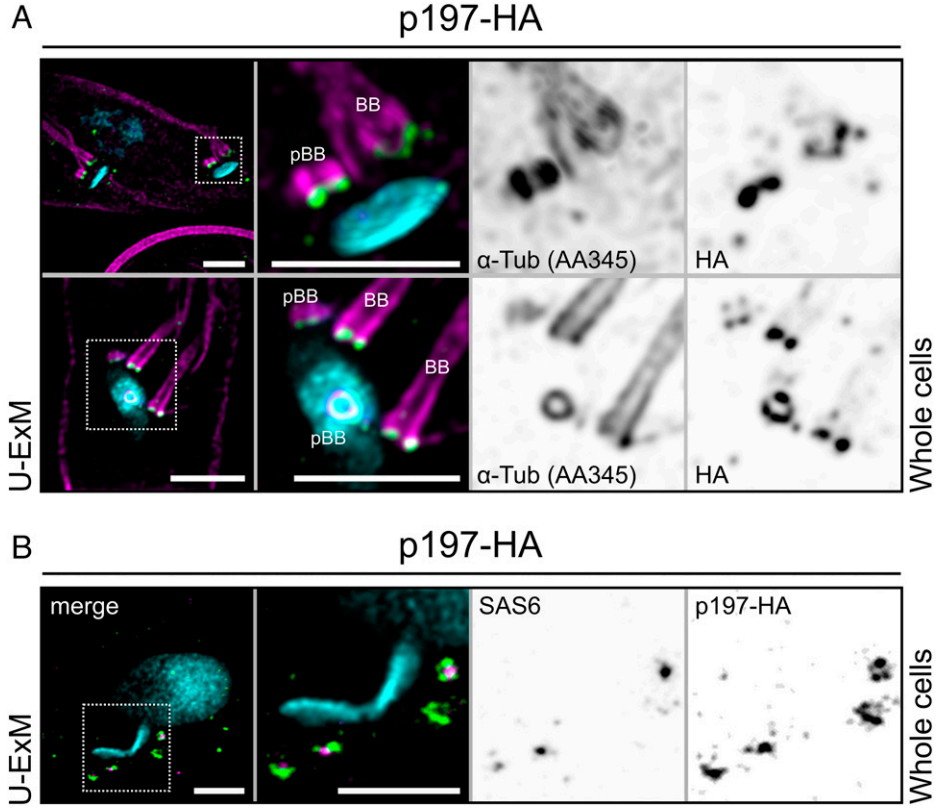

Fig. 1. p197 localizes to both the BB and pro-BB throughout the cell cycle. (*A*) U-ExM of p197-HA expressing cells stained with DAPI, the recombinant α-tubulin antibody AA345 (magenta), and for HA (green) as indicated. The *Upper* row shows a 2K1N and the lower one a dK1N cell cycle stage. (Scale bar, 2 μm.) (*B*) U-ExM as in *B* but cells were stained with DAPI (blue), for SAS6 (magenta), and HA (green). (Scale bar, 2 μm.).

aa (ΔN1228-HA). Fig. 2*A* demonstrates that expression of ΔN1228-HA cannot restore the growth inhibition caused by the absence of full-length p197. However, ΔN1228-HA correctly localizes to both the mature and the pro-BBs, stained by the α-tubulin antibody YL1/2 (Fig. 2*B* and *SI Appendix*, Fig. S3*A*), even though the cell lacks kDNA due to the absence of the TAC (Fig. 2 *B*, *Bottom*). Thus, while ΔN1228-HA cannot assemble a functional TAC the C-terminal 520 aa of p197 appear to be sufficient to associate with the mature and the pro-BBs.

To confirm and extend these results, we used the p197 3′ UTR RNAi cell line and modified one allele of p197 by in situ tagging so that it lacks the C-terminal 334 aa and contains a C-terminal HA-tag (ΔC334-HA). The resulting cell line was termed p197 3′ UTR RNA + ΔC334-HA. We observed that the ΔC334-HA variant does not restore normal growth and thus cannot functionally replace full-length p197, similar to the p197 3′ UTR RNAi + ΔN1228-HA cell line described above (Fig. 2*C*). IF analyses show that in uninduced RNAi cells expressing intact and fully functional TAC structures, ΔC334-HA is correctly localized to the BB region (Fig. 2*D* and *SI Appendix*, Fig. S3*B*). However, after 1 d of p197 RNAi induction ΔC334-HA is mainly absent from the newly formed BB, which lacks a TAC and kDNA, whereas it can still be found at the intact TAC of the old BB that is still connected to the kDNA (Fig. 2*D* and *SI Appendix*, Fig. S3*B*). After 3 d of RNAi induction, finally, when the slow growth phenotype becomes apparent and the kDNA and the TAC have been completely lost, the ΔC334-HA, while still expressed and detectable by sodium dodecyl sulfate–polyacrylamide gel electrophoresis (SDS-PAGE), is mainly absent from the BB region (Fig. 2*D* and *SI Appendix*, Fig. S3*B*). These results show that ΔC334-HA is correctly localized in the presence of an intact TAC. Thus ΔC334-HA has either retained its capability to connect to its downstream binding partner that mediates the interaction of p197 with the OM or it interacts laterally with full-length p197 present in the old TAC.

In summary, these results indicate that the C-terminal 334 to 520 aa of p197 are necessary and sufficient for the upstream association of p197 with the BBs.

The N Terminus of p197 Is Anchored at the OM. To investigate the two possibilities raised above, we generated a more drastic C-terminal deletion mutant of p197 in which 1383 aa of its C terminus were deleted. Similar to the ΔC334-HA variant the ΔC1383-HA variant is not functional yet able to correctly localize in cells that still have full-length p197 (Fig. 3 *A* and *B*). We therefore expressed the ΔC1383-HA variant in a cell line capable of inducible RNAi of the OM TAC subunit TAC40 (Fig. 3*C*). Flagella and the TAC are stable structures that remain connected to each other during a standard flagellar isolation procedure (10, 19). Fig. 3*C* shows that in the uninduced TAC40 RNAi cell line ΔC1383-HA was detected in the BB region in 80% of isolated flagella, indicating that as shown above (Fig. 3 *A* and *B*) nonfunctional ΔC1383-HA still localizes to the TAC. Ablation of TAC40 disrupts the formation of the TAC part downstream of TAC40, resulting in the delocalization of TAC components, such as p166 and TAC102 (25). Moreover, also the OM TAC subunit TAC60 and the cytosolic TAC65 that is peripherally attached to the OM get delocalized, whereas p197 remains connected to the BB (20, 25). Interestingly, in TAC40-depleted cells ΔC1383-HA was detected in only 20% of all flagella. Thus, most of ΔC1383-HA gets delocalized upon TAC40 depletion, suggesting that it binds either to TAC40 itself or to a TAC40-dependent TAC subunit such

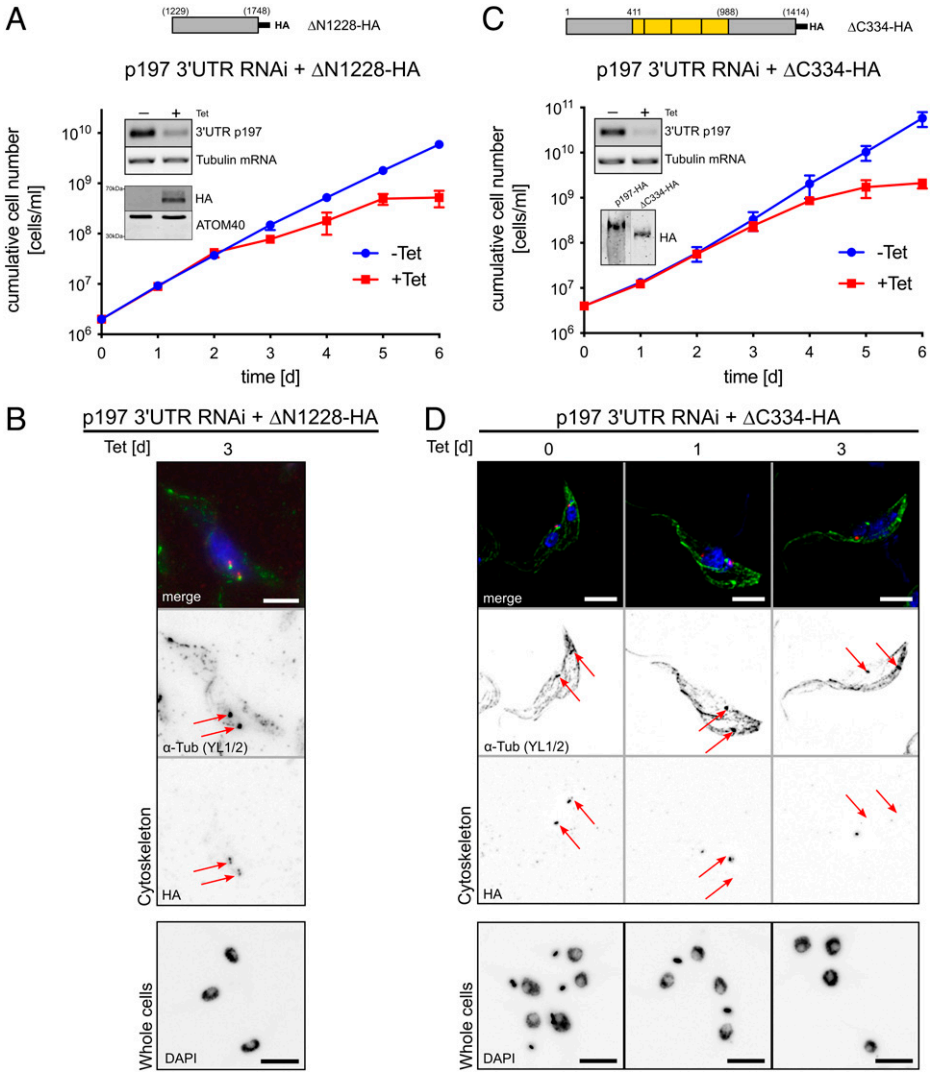

Fig. 2. The C terminus of p197 is anchored at the BB. (*A*) Growth curve of the p197 3′ UTR RNAi cell line expressing an RNAi resistant in situ C-terminally HA tagged p197 version lacking the 1228 N-terminal amino acids, termed ΔN1228-HA, schematically depicted at the *Top*. SEM ($n = 3$) are indicated. *Inset Top*: RT-PCR products of the 3′ UTR of the p197 mRNA in uninduced or 2-d induced cells. Tubulin mRNA serves as loading control. *Inset Bottom*: Immunoblot showing Tet-inducible expression of ΔN1228-HA. ATOM40 serves as loading control. (*B*) *Top* panels: IF analysis of cytoskeletons isolated from the 3-d induced cell line shown in *A* stained with DAPI (blue), the α-tubulin antibody YL1/2 (green), and for HA (red) as indicated. Red arrows indicate the positions of the two basal bodies. *Bottom* panel: IF analysis of whole cells corresponding to the *Top* panels stained with DAPI. (Scale bar, 5 μm.) (*C*) Growth curve of the p197 3′ UTR RNAi cell line expressing an RNAi resistant in situ C-terminally HA-tagged p197 version lacking the 334 C-terminal amino acids, termed ΔC334-HA, schematically depicted at the *Top*. SEM ($n = 3$) are indicated. *Inset Top*: RT-PCR products of the 3′ UTR of the p197 mRNA in uninduced or 2-d induced cells. Tubulin mRNA serves as loading control. *Inset Bottom*, immunoblot showing constitutive expression of ΔC334-HA. Full-length p197 serves as size marker for comparison. (*D*) *Top* panels: IF analysis of cytoskeletons isolated from the cell line shown in *C* stained with DAPI (blue), the α-tubulin antibody YL1/2 (green), and for HA (red) as indicated. Time of RNAi induction is indicated. Red arrows indicate the positions of the two basal bodies. *Bottom* panel: IF analysis of whole cells corresponding to the *Top* panels stained with DAPI. (Scale bar, 5 μm.) For a quantification of the IF analyses shown in *B* and *D* see *SI Appendix*, Fig. S3.

as TAC42, TAC60, and TAC65. As a control we also expressed full-length p197-HA in the TAC40 RNAi cell line and could show that its TAC localization is largely independent of TAC40 (Fig. 3*D*).

In summary, these results indicate that the N-terminal 365 aa of p197 are sufficient to anchor the protein to the mitochondrial OM. Moreover, since p197 is not affected in the TAC40 RNAi cell line we can exclude that lateral interaction with full-length p197 is responsible for localization of ΔC1383-HA to the TAC region.

The N Terminus of p197 Connects to the Peripheral OM Protein TAC65. Sequential digitonin fractionations show that p197-HA is almost exclusively recovered in the pellet 2 (P2) fraction, indicating that full-length p197 is insoluble under these conditions. HA-ΔN1228 behaves similarly, as about 70% were insoluble. For TAC40, ∼70% of the protein is released into the supernatant 2 (SN2) (Fig. 4*A* and *SI Appendix*, Fig. S4*A*). In contrast to full-length p197, nonfunctional but correctly OM-anchored ΔC1383-HA (Fig. 3), is essentially completely soluble in 1% digitonin (Fig. 4*A* and *SI Appendix*, Fig. S4*A*). It behaves similarly to the β-barrel protein ATOM40, a subunit of the mitochondrial OM protein translocase (38), which serves as a control for a digitonin-soluble complex.

To look for putative interaction partners of ΔC1383-HA we produced two cell lines coexpressing ΔC1383-HA together with either C-terminally myc-tagged TAC65 or C-terminally myc-tagged TAC60. Reciprocal coimmunoprecipitations (Co-IPs) demonstrate a stable association of TAC65-myc and ΔC1383-HA (Fig. 4*B* and *SI Appendix*, Fig. S4*B*). In contrast, ΔC1383-HA

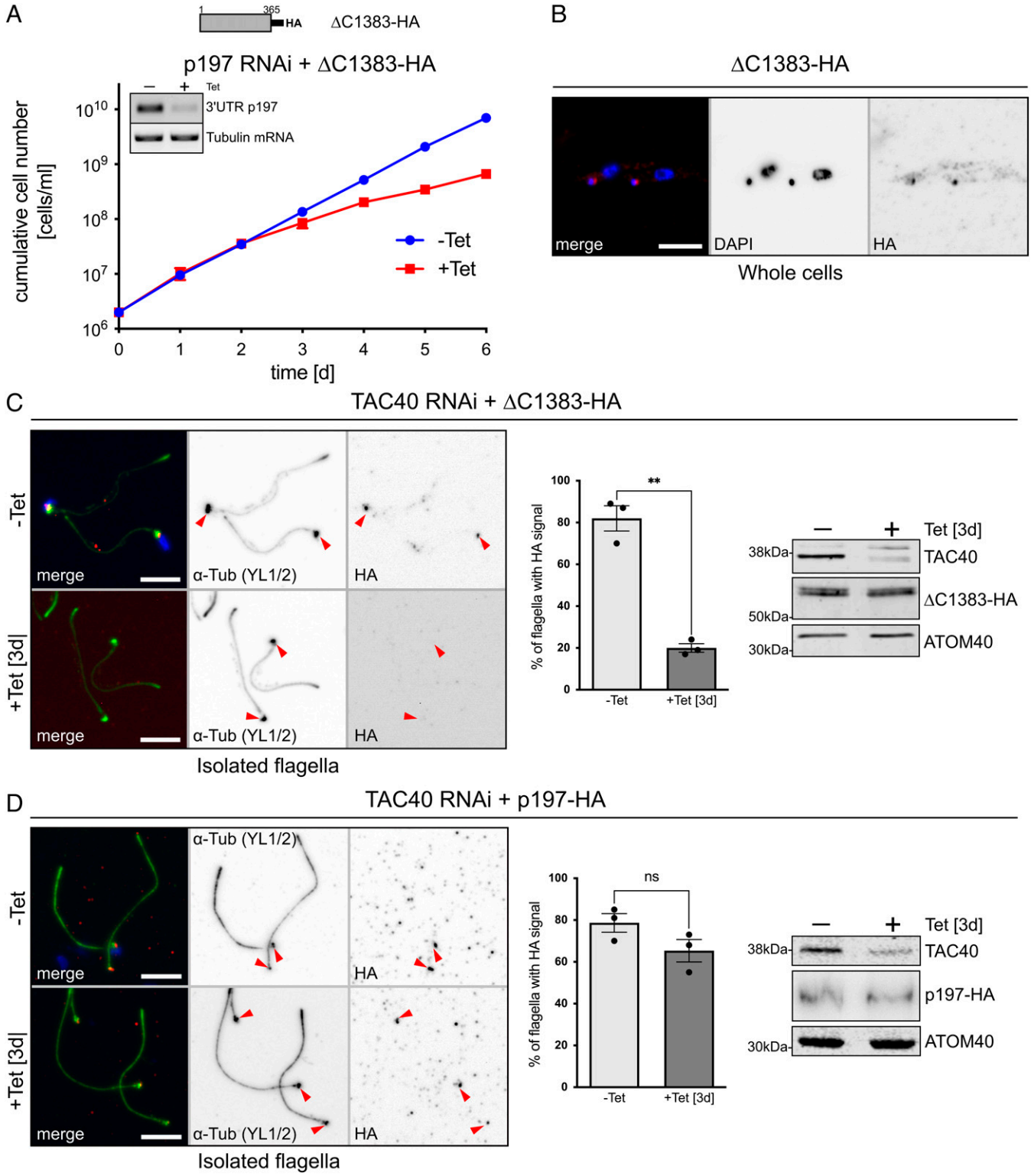

Fig. 3. The N terminus of p197 connects to the OM. (*A*) Growth curve of the p197 3′ UTR RNAi cell line expressing an RNAi resistant in situ C-terminally HA-tagged p197 version lacking the 1383 C-terminal amino acids, termed ΔC1383-HA, schematically depicted at the *Top*. SEM ($n = 3$) are indicated. *Inset Top*: RT-PCR products of the 3′ UTR of the p197 mRNA in uninduced or 2-d induced cells. Tubulin mRNA serves as loading control. (*B*) IF analysis of cells expressing ΔC1383-HA stained with DAPI (blue) and for HA (red) as indicated. (Scale bar, 5 μm.) (*C*) *Left* panels: IF analysis of isolated flagella from uninduced and 3-d induced TAC40 RNAi cell line expressing ΔC1383-HA stained with DAPI (blue), the α-tubulin antibody YL1/2 (green), and anti-HA (red) as indicated. Arrowheads point toward BBs. (Scale bar, 5 μm.) *Right* panel: Quantification of microscopic imaging results. Percentage of flagella with an HA signal was determined for three independent biological replicates. In total 574 (−Tet) and 656 (+Tet) flagella were counted. *Inset*: Immunoblot confirming ablation of TAC40 upon and constitutive expression of the ΔC1383-HA. ATOM40 serves as a loading control. (*D*) As in *C* but a TAC40 RNAi cell line expressing full-length p197-HA was analyzed. Three independent biological replicates were quantified, SEM are indicated. In total 783 (−Tet) and 612 (+Tet) flagella have been counted. For *C* and *D* an unpaired Welch's *t* test was used (**$P < 0.01$).

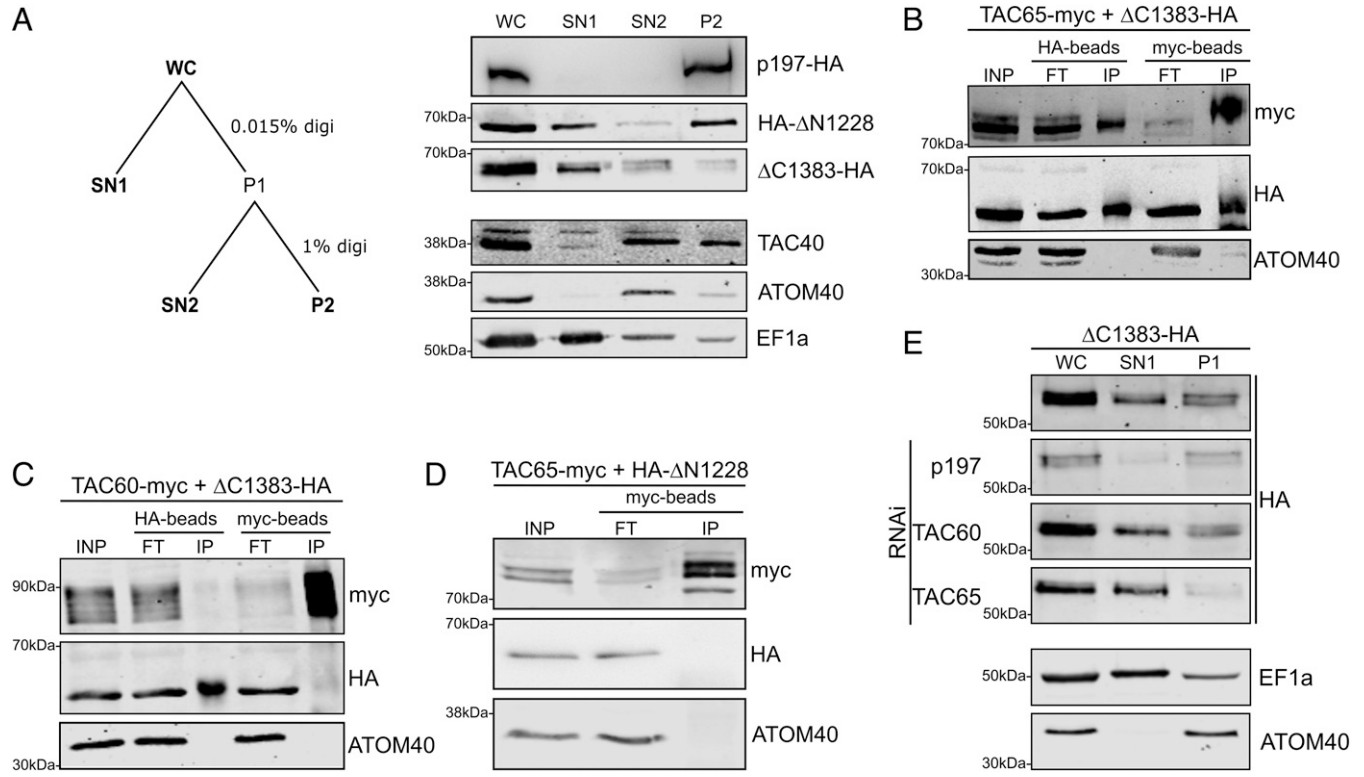

Fig. 4. The N terminus of p197 connects with TAC65. (*A*) *Left*: Outline of the digitonin fractionation analyzed by the immunoblot on the *Right*. *Right* panel: Equal cell equivalents of whole cell extract (WC), SN1, SN2, and P2 fractions of cell lines expressing p197-HA, ΔC1383-HA, and HA-ΔN1228, respectively, were separated by SDS-PAGE (4% for p197-HA and 12% for all others) and analyzed by immunoblots. EF1a, TAC40, and ATOM40 serve as cytosolic, TAC, and mitochondrial markers, respectively. Markers are shown for one cell line only. For a quantification of the immunoblots see *SI Appendix*, Fig. S4*A*. (*B* and *C*) SN2 fractions from cells coexpressing ΔC1383-HA and either TAC65-myc (*B*) or TAC60-myc (*C*) were subjected to coimmunoprecipitation using either the anti HA- or anti myc-beads as indicated. A total of 5% of input (INP) and flow through (FT) as well as 100% of the final eluate (IP) were analyzed by immunoblots probed with anti-tag antibodies. ATOM40 serves as negative control for the immunoprecipitations. For replicates of the pulldowns see *SI Appendix*, Fig. S4 *B* and *C*. (*D*) Same as *B* and *C* but whole cells coexpressing HA-ΔN1228 and TAC65-myc were directly extracted with 1% digitonin. For a replicate of the pulldown see *SI Appendix*, Fig. S4*D*. (*E*) Immunoblots containing equal cell equivalents of WC, SN1, and P1 fractions from the 2-d induced p197, TAC60, and TAC65 RNAi cell lines coexpressing ΔC1383-HA were probed for the HA-tagged p197 version and for the presence of the cytosolic and mitochondrial markers EF1a and ATOM40, respectively. For a quantification see *SI Appendix*, Fig. S4*E*.

does not pull down TAC60-myc and the reciprocal pulldown using TAC60-myc recovers only background levels of ΔC1383-HA (Fig. 4*C* and *SI Appendix*, Fig. S4*C*). Finally, we show that as expected TAC65-myc does not pull down HA-ΔN1228 as it lacks the N-terminal TAC65 binding domain (Fig. 4*D* and *SI Appendix*, Fig. S4*D*).

The hierarchical assembly model of the TAC (25) proposes that ablation of p197 results in delocalization of all downstream TAC subunits. However, putative assembly intermediates consisting of OM TAC subunits that get dispersed in the OM can still form. Evidence for such putative detergent-soluble assembly subcomplexes containing either TAC40, TAC42, and TAC60 or pATOM36 and TAC65 has been reported (20).

When cells are subjected to subcellular fractionation using a low concentration of digitonin, these OM TAC subunits (together with putative interaction partners) are mainly found in the mitochondria-enriched pellet in contrast to cytosolic proteins that are found in the supernatant. To further corroborate the interaction of ΔC1383-HA with specific OM TAC subunits, we biochemically fractionated several cell lines that express ΔC1383-HA and are capable of inducible RNAi targeting either p197, TAC60, or TAC65. In uninduced cells, substantial amounts of ΔC1383-HA are found in the pellet fraction confirming association with OM TAC subunits (Fig. 4 *E*, *Top*). Similar results are observed upon down-regulation of p197. Ablation of TAC60 leads to the release of small amounts to the soluble supernatant fraction. Strikingly, about two-thirds of ΔC1383-HA are detected in the soluble fraction in the absence of TAC65 (Fig. 4*E* and *SI Appendix*, Fig. S4*E*), which is consistent with the previous conclusion that TAC65 mediates the interaction of ΔC1383-HA with the OM.

In summary, these results strongly suggest that the N terminus of p197 is orientated toward the OM where it is likely anchored via the cytosolic and peripherally OM-associated TAC subunit TAC65. Furthermore, this proposed interaction does not require more than the N-terminal 365 aa of p197.

p197 Determines the Distance between the BB and the OM. To directly visualize that p197 bridges the distance between the OM and the BB, we made a cell line that exclusively expresses a p197 variant containing both an N-terminal myc tag and a C-terminal HA tag (*SI Appendix*, Fig. S5). This cell line, designated myc-p197-HA, grows nearly identically to wild-type cells, indicating that myc-p197-HA is fully functional (*SI Appendix*, Fig. S6*A*). We then used U-ExM to localize the N and C termini of p197 relative to the OM and BB. The results show approximate colocalization of the OM marker ATOM40 with the N terminus of p197 (Fig. 5 *A*, *Top*), whereas the C terminus of p197 is found adjacent to the base of the BB (Fig. 5 *B*, *Top*). Quantification revealed that the length of p197, and thus the median distance bridged by p197 (measured in Fig. 5 *B*, *Top*), is 200 nm (Fig. 5 *C*, *Left* lane).

The central region of p197 consists of nearly identical 175-aa repeats, the exact number of which is difficult to determine

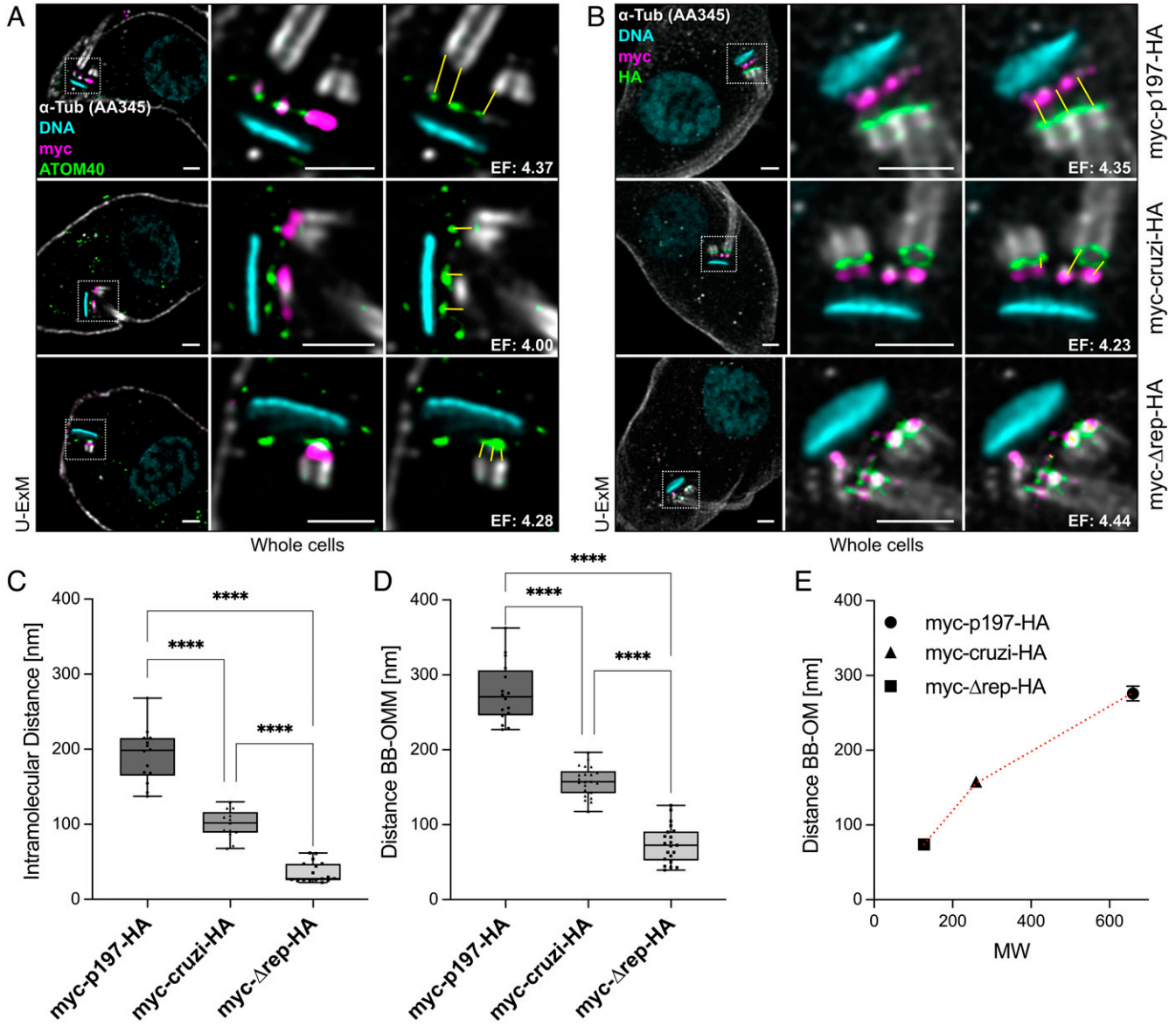

Fig. 5. p197 is the exclusion zone filament. (*A*) U-ExM of a cell line exclusively expressing myc-p197-HA (*Top* panels). U-ExM of p197 3′ UTR RNAi cell lines expressing either myc-cruzi-HA (2-d induced, *Middle* panels) or myc-Δrep-HA (1-d induced, *Bottom* panels), respectively. Cells were stained with DAPI (magenta), the recombinant α-tubulin antibody AA345 (white), for myc (pink) and for ATOM40 (green) as indicated. One plane of the imaged z-stack is shown. *Right* two panels: *Inset* of *Left* panels. Yellow lines indicate the measured distances. Average of the three distances has been taken as one data point for the quantification in *D*. Expansion factors (EFs) are indicated. (Scale bar, 2 μm.) (*B*) U-ExM as in *A* but cells were stained with DAPI (magenta), the recombinant α-tubulin antibody AA345 (white), for HA (green), and for myc (pink) as indicated. Z-stack projections of the z-stack are shown. (*C* and *D*) Boxplot of the distances between HA and myc measured in *B* (n = 14, 17, 13) and tubulin and ATOM40 measured in *A* (n = 16, 22, 21), respectively. Measured distances in U-ExM pictures were divided by the corresponding EF for the graphs. An ordinary one-way ANOVA test with post hoc Tukey's honest significance test (****$P < 0.0001$). (*E*) Data points of the mean distances between BB and OM have been plotted against the predicted molecular weights (MWs) of the three p197 variants. SEM is indicated.

because they often lead to errors in genome assembly (39). A recent sequencing of the genome of the *T. b. brucei* strain EATRO1125 indicates that p197 has ∼26 repeats (40), suggesting a molecular mass of the protein of 660 kDa. Thus, p197 may be one of the largest trypanosomal proteins known. This is also true for *T. brucei* strain 427 used in the present study, as shown by SDS-PAGE, where p197 migrates much slower than the marker with the highest molecular weight of 260 kDa (*SI Appendix*, Fig. S1*C*). Therefore, we assume that 660 kDa is a reasonable estimate for the molecular mass of full-length p197.

Next, we investigated whether the distance between the BB and the mitochondrial OM is determined by the length of p197 and how this distance affects cell growth. To this end, we generated two cell lines expressing shorter versions of p197 in the background of the induced p197 3′ UTR RNAi cell line. The first, myc-Δrep-HA, lacks the entire α-helical repeat domain and has a molecular mass of 127 kDa. In the second, we replaced the repeat domain of *T. brucei* p197 with the corresponding α-helical region of the *Trypanosoma cruzi* p197 ortholog, which lacks the repeats. The *T. cruzi* region was used because it is technically very challenging to delete a defined number of repeats from *T. brucei* p197. The resulting medium length version of p197 was designated myc-cruzi-HA and has a molecular mass of 260 kDa. Neither of the two shorter versions of p197 was able to complement the growth arrest of the p197-3′ UTR RNAi cell line, although the cell line complemented with the longer myc-cruzi-HA grew slightly better (*SI Appendix*, Fig. S6 *B* and *C*). Note that myc-p197-HA

and myc-cruzi-HA are expressed at similar levels but only the full-length protein allows normal growth (*SI Appendix*, Fig. S6*D*).

However, the N termini of both p197 versions were still in close vicinity with ATOM40, and their C termini were adjacent to the BB, as was the case with the full-length protein (Fig. 5 *A* and *B*). Intriguingly, expression of the two shorter p197 versions in the induced p197 3′ UTR RNAi cell line resulted in a reduced distance between the OM marker ATOM40 and the α-tubulin–stained BB, when compared to wild-type cells (Fig. 5*D*), which was proportional to the molecular weight of the shorter variants and thus to their lengths (Fig. 5*E*). Thus, we conclude that the EZFs of the TAC are formed by p197: The N terminus faces the OM and the C terminus interacts with the BB. The length of p197 molecules determines the mean length of the EZFs. The fact that the repeat domain of the p197 of *T. brucei* could be replaced by the central domain of its *T. cruzi* ortholog, which has no repeats, suggests that an α-helical structure of this region is sufficient to link the two structures. Finally, a minimal length of EZFs seems to be crucial, since two shorter versions of p197 are still able to connect the OM to the BB but cannot support TAC function.

Discussion

Here, we show that the EZFs of the TAC consist of filaments, likely made of single p197 molecules, spanning the region between the BBs and the periphery of the OM (see model Fig. 6). Assembly of these filaments starts very early in the cell cycle, immediately after the formation of a new pro-BB before the new flagellum starts to grow.

p197 can be divided into three domains: the N-terminal, the C-terminal, and the central region, all of which have distinct functions and are required for an intact TAC.

The N terminus of p197 is anchored to the OM by binding to TAC65, which in turn interacts with the OM integral TAC subunit pATOM36 (see model Fig. 6). TAC65 was first identified in a pull-down experiment of tagged pATOM36 that also recovered p197. Pull-down analysis using tagged TAC65 as a bait recovered pATOM36, suggesting that TAC65 and pATOM36 form a complex that likely also contains p197 (20).

U-ExM indicates that the C terminus of p197 originates from or in the vicinity of the ring defined by the nine triplet microtubules at the bottom of the mature and the pro-BB, suggesting that p197 is the TAC subunit most proximal to the BB. However, which BB component exactly the C-terminal region of p197 binds to remains to be determined.

How intracellular structures are arranged and how far apart they are, are important geometric properties for cellular function (41). The EZF region of the TAC is an excellent example as it sets the distance between the OM and the BB at a median of 270 nm. Here we show that this distance is directly determined by the length of single or parallel bundles of p197 molecules. Replacing full-length p197 (estimated to be 660 kDa) with the two shorter versions myc-cruzi-HA (260 kDa) and myc-Δrep-HA (127 kDa), shortens the distance between the OM and the BB proportionally (Fig. 5*E*). These results would be consistent with the concept of a molecular ruler in which a single linear coiled-coil protein determines the length of a polymeric structure (42). However, if p197 indeed functions as a molecular ruler, we must postulate that the ULFs contain a polymeric structure. Currently, there is no evidence for this. Using a single coiled-coil spacer protein to define the OM–BB distance appears to be sufficient for p197 function. In fact, a complex polymeric structure that includes p197 as a molecular ruler might be too rigid. Instead we favor that p197 acts as a monomolecular spacer element that does not require additional factors.

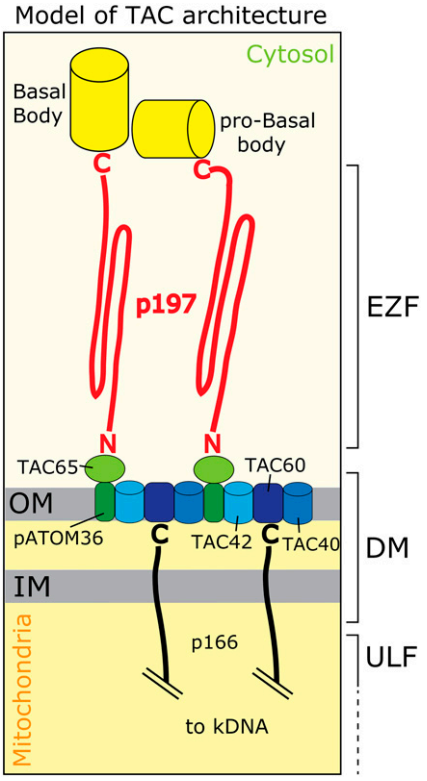

Fig. 6. Model depicting the architecture of the EZF and the DM region of the trypanosomal TAC. p197 likely is the TAC subunit most proximal to the BB. One p197 molecule (red) each that connects either the BB or the pro-BB to the OM is shown. The C terminus of p197 interacts with the BB or the pro-BB and its N terminus binds to the cytosolic membrane peripheral TAC65. p197 is predicted to have a high α-helical content, which likely forms coiled-coil domains containing multiple α-helices. TAC65 and pATOM36 form a subcomplex in OM that is indicated in green. TAC60, TAC42, and TAC40, the latter two of which are β-barrel proteins, from a second OM subcomplex, depicted in blue. p166 interacts with TAC60 via its C terminus. It has a single transmembrane domain and likely is the only TAC subunit integral to the IM. Thus, the TAC65/pATOM36 and the TAC60/TAC42/TAC40 subcomplexes form a platform in the OM that integrates the EZFs with the intramitochondrial ULFs. How the ULFs connect to the kDNA is not shown.

Interestingly, other macromolecular structures mediating segregation of nuclear genomes do also contain spacer proteins. Examples include yeast SPC110, which precisely determines the distance between the central and the inner plaques of the spindle pole body to ∼40 nm (43), and the synaptonemal complex of yeast, where an antiparallel assembly of Zip1 proteins fix the distance between homologous chromosomes to ∼115 nm (44). Intriguingly, p197 bridges a median distance of ∼200 nm (Fig. 5*C*), which is much longer than is observed in the other examples.

Our study not only shows that p197 determines the distance between the OM and BB but also that this distance is important for TAC function. While the two shorter p197 versions can still connect the two structures, the much shorter OM–BB distance prevents normal cell growth (*SI Appendix*, Fig. S6). The reason for this could be that the orientations of the old and the new mature and pro-BB are dynamic and sometimes perpendicular to each other. During each cell cycle, the new

mature BB rotates counterclockwise around the old flagellum (45). It could be this dance of the BBs that requires their attachments to the OM to be very flexible and to exceed a certain minimal length.

The Phyre2 algorithm predicts that the repeat domain of p197 has an α-helical content of 96% (*SI Appendix*, Fig. S7*A*). Considering its molecular weight of 660 kDa and assuming p197 consists mainly of α-helices, it could span a maximum distance of 853 nm (3.6 aa/0.54 nm per helix turn). This is very close to the median distance from the myc to the HA tag of full-length p197 of ∼860 nm as measured after U-ExM. The fact that the median distance between the OM and the BB after U-ExM is 1,100 nm and therefore longer than p197 can be explained by the fact that the p197 N terminus does not directly interact with the OM but binds to the peripheral OM protein TAC65, and that we do not know which exact region of the BB p197 binds to.

The U-ExM protocol used in our study did not involve protease treatment. Our results therefore also illustrate the power of U-ExM, which in the case of p197 is able to spatially resolve different domains within single intact molecules. This suggests that the expansion polymer in U-ExM is very uniformly distributed, allowing for high precision expansion.

Assuming an α-helical structure, p197 is long enough to span the distance between the OM/TAC65 and the BB more than four times in living cells. However, because the diameter of the EZF filaments was estimated to be between 5 and10 nm (15), which is larger than the 1.2-nm diameter of an average α-helix, it is likely that p197 adopts a higher order structure such as coiled-coil domains.

The kDNA and its connection to the flagellum via the TAC is a defining feature of the *Kinetoplastidae* and orthologs of p197 are found in essentially all Kinetoplastids. A multiple sequence alignment of p197 with a group of diverse Kinetoplastids comprising *T. brucei*, *T. cruzi*, *Leishmania major*, and *Paratrypanosoma confusum* revealed that the N-terminal 150 aa as well as the 60 aa of the very C terminus are more conserved than the central region of the protein (*SI Appendix*, Fig. S8). The N-terminal region of p197 (amino acids 26 to 78) contains a zinc-finger domain that is conserved in most p197 orthologs. Its relevance is presently unknown. All p197 orthologs are of high predicted molecular mass and have a very high predicted α-helical content in their central regions (*SI Appendix*, Fig. S7*B*). However, while *T. brucei* p197 contains nearly identical repeats, no such repeats are found in the central region of p197 orthologs of other Kinetoplastids. The N and C termini of p197 are involved in protein–protein interactions with the OM and the BB, respectively. This may explain why these regions are under a stronger selection pressure and more conserved than the diverged central part. The latter is under less constraints because it likely needs to simply provide an α-helical flexible spacer of sufficient length.

Materials and Methods

Transgenic Cell Lines. All cell lines derive from *T. brucei* 427. Tet-inducible RNAi of p197 (Tb927.10.15750) targets the 424-nt-long 3′ UTR of the p197 mRNA. PCR-based in situ N-terminal myc tagging of p197 and its variants was done with primers defining the flanking region of the start codon. The plasmid for amplification was a derivative of the pN-PURO-PTP (46). PCR-based in situ C-terminal HA tagging of p197 and its variants was done using plasmids of the pMOtag series as templates (47). TAC65-myc and TAC60-myc were generated with a modified pLew100 expression vector (48). For p197 truncations, PCR products corresponding to the ORF that either lacked the first 1228 or the last 1383 aa were amplified and integrated into the vector allowing for C-terminal triple HA tagging.

To test functionality of double-tagged p197, a plasmid for the single knockout of p197 was generated by modification of a pMOtag43M vector (47). The 5′ and the 3′ flanking sequence were amplified and ligated into the vector, thereby flanking the hygromycin resistance gene. To generate the myc-Δrep-HA variant construct the region of the gene corresponding to the N terminus was amplified and cloned into a vector for N-terminal myc tagging. The region corresponding to the C-terminal part was amplified accordingly and integrated into a vector for C-terminal HA tagging. Finally, the two fragments were fused producing the myc-Δrep-HA gene. This construct was then used to insert the α-helical stretch of the *T. cruzi* p197 gene to generate a construct encoding the myc-cruzi-HA version. For details see *SI Appendix*, which also contains on overview of all p197 variants used in *SI Appendix*, Fig. S9 and Table S1.

Immunofluorescence Microscopy. For whole cell IF analysis parasites were fixed using 4% paraformaldehyde (PFA) and permeabilized with 0.2% Triton X-100. For cytoskeletons, cells were permeabilized with 0.05% Triton X-100 and then fixed with 4% PFA. Flagella were isolated as described (49) and fixed with 4% PFA.

Primary antibodies were diluted in phosphate-buffered saline (PBS) containing 2% bovine serum albumin (BSA), secondary fluorescent antibodies in PBS only. Z-stack images were acquired using a DMI6000B microscope equipped with a DFC360 FX monochrome camera and LAS X software (Leica Microsystems). For details see *SI Appendix*.

U-ExM. Cells on coverslips are transferred into FAB solution (0.7% formaldehyde [36.5 to 38%] and 1% acrylamide 40% in PBS) and incubated for 5 h at 37 °C. One drop of monomer solution containing 19% sodium acrylate, 10% (wt/wt) acrylamide, and 0.1% (wt/wt) N,N′-methylenebisacrylamide in PBS supplemented with 0.5% ammoniumpersulfate and 0.5% tetramethylethylendiamine was placed on the parafilm. Coverslips were put on the drop. After gelation, samples were incubated at 37 °C in the dark. Coverslips were then transferred into denaturation buffer (200 mM SDS, 200 mM NaCl, and 50 mM Tris, pH 9) to allow the gel to detach from the coverslip. Gels were incubated in denaturation buffer at 95 °C and placed in water for a first round of expansions and incubated overnight. Subsequently, gels were washed and incubated with the primary antibody. After washing in 0.1% PBS-Tween 20 gels were incubated with secondary antibodies. Finally they were washed again and placed in water for expansion. For details see *SI Appendix*.

Mounting and Image Acquisition. A gel piece is mounted on a poly-D-lysine coverslip and gently pressed with a brush to ensure adherence of the gel to the coverslip. Confocal microscopy is performed on a Leica TCS SP8 using a 63 × 1.4 numerical aperture (NA) oil objective. LAS X software (Leica Microsystems), Huygens Professionals, ImageJ and Prism were used to analyze the images. For details see *SI Appendix*.

Calculation of Expansion Factors from U-ExM. The expansion factor for single-tagged p197 (Fig. 1) was determined by measuring the lengths of the cell, the kDNA, and the diameter of the nucleus before and after expansion. The expansion factor for images from the p197 double-tagged cell lines (Fig. 5) were calculated based on basal body diameter. For details see *SI Appendix*.

Cell Fractionation. Two-step digitonin extractions were performed to analyze the subcellular localization of proteins. Washed cells were extracted in SoTE buffer (20 mM Tris HCl pH 7.5, 0.6 M sorbitol, 2 mM ethylenediaminetetraacetic acid (EDTA)) containing 0.03% (wt/vol) digitonin. The sample was centrifuged and the pellet extracted again with 1% digitonin. Equal cell equivalents of all fractions were analyzed using SDS-PAGE. For details see *SI Appendix*.

Immunoprecipitations. For immunoprecipitation of the ΔC1383 variant a mitochondria-enriched pellet was solubilized in lysis buffer (20 mM Tris HCl pH 7.4, 100 mM NaCl, 0.1 mM EDTA, 10% glycerol) containing 1% digitonin. For immunoprecipitation of the ΔN1228 variant, whole cells were solubilized in lysis buffer containing 1% digitonin. All samples were centrifuged and half of the supernatant was either incubated with anti-c myc beads or anti-HA beads, respectively. Beads were eluted by boiling in SDS-PAGE sample buffer lacking β-mercaptoethanol. All fractions were subjected to immunoblot analysis. For details see *SI Appendix*.

Miscellaneous. Immunoblots and Northern blots were done as previously described (50). RT-PCR of the 3′ UTR of the p197 mRNA was done to determine the efficiencies of the various p197 RNAi cell lines. For details see *SI Appendix*. For a list of antibodies used in the study see *SI Appendix*.

Data, Materials, and Software Availability. All study data are included in the article and/or supporting information.

ACKNOWLEDGMENTS. Work in the laboratory of A.S. was supported in part by the National Centre of Competence in Research: RNA and Disease (grant nos. 182880 and 205601) and by project grant SNF 175563 both funded by the Swiss National Science Foundation. The T.O. laboratory is supported by a grant from the Swiss National Science Foundation (SNF 179454) and the Uniscientia Foundation.

1. C. M. Gustafsson, M. Falkenberg, N. G. Larsson, Maintenance and expression of mammalian mitochondrial DNA. *Annu. Rev. Biochem.* **85**, 133–160 (2016).
2. B. Westermann, Mitochondrial inheritance in yeast. *Biochim. Biophys. Acta* **1837**, 1039–1046 (2014).
3. Z. Verner *et al.*, Malleable mitochondrion of *Trypanosoma brucei*. *Int. Rev. Cell Mol. Biol.* **315**, 73–151 (2015).
4. A. Schneider, Unique aspects of mitochondrial biogenesis in trypanosomatids. *Int. J. Parasitol.* **31**, 1403–1415 (2001).
5. R. E. Jensen, P. T. Englund, Network news: The replication of kinetoplast DNA. *Annu. Rev. Microbiol.* **66**, 473–491 (2012).
6. M. L. Povelones, Beyond replication: Division and segregation of mitochondrial DNA in kinetoplastids. *Mol. Biochem. Parasitol.* **196**, 53–60 (2014).
7. R. J. Wheeler, K. Gull, J. D. Sunter, Coordination of the cell cycle in trypanosomes. *Annu. Rev. Microbiol.* **73**, 133–154 (2019).
8. K. M. Tyler, K. R. Matthews, K. Gull, Anisomorphic cell division by African trypanosomes. *Protist* **152**, 367–378 (2001).
9. A.-L. Chanez, A. B. Hehl, M. Engstler, A. Schneider, Ablation of the single dynamin of *T. brucei* blocks mitochondrial fission and endocytosis and leads to a precise cytokinesis arrest. *J. Cell Sci.* **119**, 2968–2974 (2006).
10. D. R. Robinson, K. Gull, Basal body movements as a mechanism for mitochondrial genome segregation in the trypanosome cell cycle. *Nature* **352**, 731–733 (1991).
11. A. Schneider, T. Ochsenreiter, Failure is not an option–Mitochondrial genome segregation in trypanosomes. *J. Cell Sci.* **131**, jcs221820 (2018).
12. J. Blanco-Ameijeiras, P. Lozano-Fernández, E. Martí, Centrosome maturation–In tune with the cell cycle. *J. Cell Sci.* **135**, jcs259395 (2022).
13. P. Ťumová *et al.*, Inheritance of the reduced mitochondria of *Giardia intestinalis* is coupled to the flagellar maturation cycle. *BMC Biol.* **19**, 193 (2021).
14. A. Regoes *et al.*, Protein import, replication, and inheritance of a vestigial mitochondrion. *J. Biol. Chem.* **280**, 30557–30563 (2005).
15. E. O. Ogbadoyi, D. R. Robinson, K. Gull, A high-order trans-membrane structural linkage is responsible for mitochondrial genome positioning and segregation by flagellar basal bodies in trypanosomes. *Mol. Biol. Cell* **14**, 1769–1779 (2003).
16. Z. Zhao, M. E. Lindsay, A. Roy Chowdhury, D. R. Robinson, P. T. Englund, p166, a link between the trypanosome mitochondrial DNA and flagellum, mediates genome segregation. *EMBO J.* **27**, 143–154 (2008).
17. B. Schimanski *et al.*, p166 links membrane and intramitochondrial modules of the trypanosomal tripartite attachment complex. *PLoS Pathog.* **18**, e1010207 (2022).
18. R. Trikin *et al.*, TAC102 is a novel component of the mitochondrial genome segregation machinery in trypanosomes. *PLoS Pathog.* **12**, e1005586 (2016).
19. F. Schnarwiler *et al.*, Trypanosomal TAC40 constitutes a novel subclass of mitochondrial β-barrel proteins specialized in mitochondrial genome inheritance. *Proc. Natl. Acad. Sci. U.S.A.* **111**, 7624–7629 (2014).
20. S. Käser *et al.*, Biogenesis of the mitochondrial DNA inheritance machinery in the mitochondrial outer membrane of *Trypanosoma brucei*. *PLoS Pathog.* **13**, e1006808 (2017).
21. S. Käser *et al.*, Outer membrane protein functions as integrator of protein import and DNA inheritance in mitochondria. *Proc. Natl. Acad. Sci. U.S.A.* **113**, E4467–E4475 (2016).
22. K. Stefan Dimmer, D. Rapaport, The enigmatic role of Mim1 in mitochondrial biogenesis. *Eur. J. Cell Biol.* **89**, 212–215 (2010).
23. D. G. Vitali *et al.*, Independent evolution of functionally exchangeable mitochondrial outer membrane import complexes. *eLife* **7**, e34488 (2018).
24. L. Gheiratmand, A. Brasseur, Q. Zhou, C. Y. He, Biochemical characterization of the bi-lobe reveals a continuous structural network linking the bi-lobe to other single-copied organelles in *Trypanosoma brucei*. *J. Biol. Chem.* **288**, 3489–3499 (2013).
25. A. Hoffmann *et al.*, Molecular model of the mitochondrial genome segregation machinery in *Trypanosoma brucei*. *Proc. Natl. Acad. Sci. U.S.A.* **115**, E1809–E1818 (2018).
26. I. Vakonakis, The centriolar cartwheel structure: Symmetric, stacked, and polarized. *Curr. Opin. Struct. Biol.* **66**, 1–7 (2021).
27. J. C. de Leon *et al.*, A SAS-6-like protein suggests that the Toxoplasma conoid complex evolved from flagellar components. *Eukaryot. Cell* **12**, 1009–1019 (2013).
28. H. Hu, Y. Liu, Q. Zhou, S. Siegel, Z. Li, The centriole cartwheel protein SAS-6 in *Trypanosoma brucei* is required for probasal body biogenesis and flagellum assembly. *Eukaryot. Cell* **14**, 898–907 (2015).
29. K. T. M. Pham, Z. Li, Regulated protein stabilization underpins the functional interplay among basal body components in *Trypanosoma brucei*. *J. Biol. Chem.* **295**, 729–742 (2020).
30. D. H. Lai, F. Moreira-Leite, Z. S. Xu, J. Yang, K. Gull, A specific basal body linker protein provides the connection function for basal body inheritance in trypanosomes. *Proc. Natl. Acad. Sci. U.S.A.* **118**, e2014040118 (2021).
31. A. Kalichava, T. Ochsenreiter, Ultrastructure expansion microscopy in *Trypanosoma brucei*. *Open Biol.* **11**, 210132 (2021).
32. P. Gorilak *et al.*, Expansion microscopy facilitates quantitative super-resolution studies of cytoskeletal structures in kinetoplastid parasites. *Open Biol.* **11**, 210131 (2021).
33. S. Amodeo *et al.*, Characterization of the novel mitochondrial genome segregation factor TAP110 in *Trypanosoma brucei*. *J. Cell Sci.* **134**, jcs254300 (2021).
34. E. D. Karagiannis, E. S. Boyden, Expansion microscopy: Development and neuroscience applications. *Curr. Opin. Neurobiol.* **50**, 56–63 (2018).
35. A. T. Wassie, Y. Zhao, E. S. Boyden, Expansion microscopy: Principles and uses in biological research. *Nat. Methods* **16**, 33–41 (2019).
36. A. Guerreiro, P. Meraldi, AA344 and AA345 antibodies recognize the microtubule network in human cells by immunofluorescence. *Antibody Reports* **2**, e17 (2019).
37. T. Sherwin, A. Schneider, R. Sasse, T. Seebeck, K. Gull, Distinct localization and cell cycle dependence of COOH terminally tyrosinolated alpha-tubulin in the microtubules of *Trypanosoma brucei brucei*. *J. Cell Biol.* **104**, 439–446 (1987).
38. M. Pusnik *et al.*, Mitochondrial preprotein translocase of trypanosomatids has a bacterial origin. *Curr. Biol.* **21**, 1738–1743 (2011).
39. O. K. Tørresen *et al.*, Tandem repeats lead to sequence assembly errors and impose multi-level challenges for genome and protein databases. *Nucleic Acids Res.* **47**, 10994–11006 (2019).
40. A. Naguleswaran *et al.*, Developmental changes and metabolic reprogramming during establishment of infection and progression of *Trypanosoma brucei brucei* through its insect host. *PLoS Negl. Trop. Dis.* **15**, e0009504 (2021).
41. W. F. Marshall, How cells measure length on subcellular scales. *Trends Cell Biol.* **25**, 760–768 (2015).
42. I. Katsura, Determination of bacteriophage lambda tail length by a protein ruler. *Nature* **327**, 73–75 (1987).
43. J. V. Kilmartin, S. L. Dyos, D. Kershaw, J. T. Finch, A spacer protein in the *Saccharomyces cerevisiae* spindle poly body whose transcript is cell cycle-regulated. *J. Cell Biol.* **123**, 1175–1184 (1993).
44. K. S. Tung, G. S. Roeder, Meiotic chromosome morphology and behavior in zip1 mutants of *Saccharomyces cerevisiae*. *Genetics* **149**, 817–832 (1998).
45. S. Vaughan, K. Gull, Basal body structure and cell cycle-dependent biogenesis in *Trypanosoma brucei*. *Cilia* **5**, 5 (2016).
46. B. Schimanski, T. N. Nguyen, A. Günzl, Highly efficient tandem affinity purification of trypanosome protein complexes based on a novel epitope combination. *Eukaryot. Cell* **4**, 1942–1950 (2005).
47. M. Oberholzer, S. Morand, S. Kunz, T. Seebeck, A vector series for rapid PCR-mediated C-terminal in situ tagging of *Trypanosoma brucei* genes. *Mol. Biochem. Parasitol.* **145**, 117–120 (2006).
48. E. Wirtz, S. Leal, C. Ochatt, G. A. Cross, A tightly regulated inducible expression system for conditional gene knock-outs and dominant-negative genetics in *Trypanosoma brucei*. *Mol. Biochem. Parasitol.* **99**, 89–101 (1999).
49. R. Sasse, K. Gull, Tubulin post-translational modifications and the construction of microtubular organelles in *Trypanosoma brucei*. *J. Cell Sci.* **90**, 577–589 (1988).
50. J. Mani *et al.*, Mitochondrial protein import receptors in Kinetoplastids reveal convergent evolution over large phylogenetic distances. *Nat. Commun.* **6**, 6646 (2015).